

Probing anomalous quartic $\gamma\gamma\gamma\gamma$ couplings in light-by-light collisions at the CLIC

S.C. İnan*

Department of Physics, Sivas Cumhuriyet University, 58140, Sivas, Turkey

and

A.V. Kisselev†

Division of Theoretical Physics, A.A. Logunov Institute for High Energy Physics,

NRC “Kurchatov Institute”, 142281, Protvino, Russia

Abstract

The anomalous quartic neutral couplings of the $\gamma\gamma\gamma\gamma$ vertex in a polarized light-by-light scattering of the Compton backscattered photons at the CLIC are examined. Both differential and total cross sections are calculated for e^+e^- collision energies 1500 GeV and 3000 GeV. The helicity of the initial electron beams is taken to be ± 0.8 . The unpolarized and SM cross sections for the same values of helicities are also estimated. The 95% C.L. exclusion limits on two anomalous photon couplings ζ_1 and ζ_2 are calculated. The best bounds on these couplings are found to be $4.58 \times 10^{-16} \text{ GeV}^{-4}$ and $9.37 \times 10^{-16} \text{ GeV}^{-4}$, respectively. The results are compared with the exclusion bounds obtained previously for the LHC. It is shown that the light-by-light scattering at the CLIC has a greater potential to search for the anomalous quartic neutral couplings of the $\gamma\gamma\gamma\gamma$ vertex.

1 Introduction

In the Standard Model (SM), the trilinear gauge couplings (TGCs) [1, 2] and quartic gauge couplings (QGCs) [3]-[5] are completely defined by the

*Electronic address: sceminan@cumhuriyet.tr

†Electronic address: alexandre.kisselev@ihep.ru

non-Abelian $SU(2)_L \times U(1)_Y$ gauge symmetry. These couplings have been accurately tested by experiments. A possible deviation from the electroweak predictions can give us important information on probable physics beyond the SM.

Anomalous TGCs and QGCs can be studied in a model independent way in the framework of the effective field theory (EFT) via Lagrangian [6]-[8]

$$\mathcal{L}_{\text{eff}} = \mathcal{L}_{\text{SM}} + \mathcal{L}_{(6)} + \mathcal{L}_{(8)}. \quad (1)$$

The Lagrangian $\mathcal{L}_{(6)}$ contains dimension-6 operators. It generates an anomalous contribution to the TGCs and QGCs. Let us underline that the lowest dimension operators that modify the quartic gauge interactions without exhibiting two or three weak gauge boson vertices are dimension-8. The Lagrangian $\mathcal{L}_{(8)}$ is a sum of dimension-8 genuine operators,

$$\mathcal{L}_{(8)} = \sum_i \frac{c_i}{\Lambda^4} \mathcal{O}_i^{(8)}, \quad (2)$$

where Λ is a mass-dimension scale associated with new physics, and c_i are dimensionless constants. This Lagrangian induces anomalous deviation to the QGCs. It is assumed that the new interaction respects the local $SU(2)_L \times U(1)_Y$ symmetry which is broken spontaneously by the vacuum expectation value of the Higgs field Φ . CP invariance is also imposed. It means that $\mathcal{L}_{(8)}$ is invariant under the full gauge symmetry. As a result, the electroweak gauge bosons can appear in the operators $\mathcal{O}_i^{(8)}$ only from covariant derivatives of the Higgs doublet $D_\mu \Phi$ or from the field strengths $B_{\mu\nu}, W_{\mu\nu}^a$.

There are three classes of dimension-8 operators. The first one contains just $D_\mu \Phi$. It leads to non-standard quartic couplings of massive vector bosons, $W^+W^-W^+W^-$, W^+W^-ZZ and $ZZZZ$. The second class contains two $D_\mu \Phi$ and two field strength tensors. The third class has four field strength tensors only. The dimension-8 operators of these two classes induce the anomalous quartic neutral couplings of the vertices $\gamma\gamma\gamma\gamma$, $\gamma\gamma\gamma Z$, $\gamma\gamma ZZ$, γZZZ , and $ZZZZ$. A complete list of dimension-8 operators which lead to anomalous quartic neutral gauge boson couplings is presented in [9]-[11]. In particular, the effective Lagrangian of the operators $\mathcal{O}_i^{(8)}$ which contributes

to the anomalous quartic couplings of the vertex $\gamma\gamma\gamma\gamma$ looks like

$$\begin{aligned}\mathcal{L}_{\text{QNGC}} = & \frac{c_8}{\Lambda^4} B_{\rho\sigma} B^{\rho\sigma} B_{\mu\nu} B^{\mu\nu} + \frac{c_9}{\Lambda^4} W_{\rho\sigma}^a W^{a\rho\sigma} W_{\mu\nu}^b W^{b\mu\nu} + \frac{c_{10}}{\Lambda^4} W_{\rho\sigma}^a W^{b\rho\sigma} W_{\mu\nu}^a W^{b\mu\nu} \\ & + \frac{c_{11}}{\Lambda^4} B_{\rho\sigma} B^{\rho\sigma} W_{\mu\nu}^a W^{a\mu\nu} + \frac{c_{13}}{\Lambda^4} B_{\rho\sigma} B^{\sigma\nu} B_{\nu\mu} B^{\mu\rho} + \frac{c_{14}}{\Lambda^4} W_{\rho\sigma}^a W^{a\sigma\nu} W_{\nu\mu}^b W^{b\mu\rho} \\ & + \frac{c_{15}}{\Lambda^4} W_{\rho\sigma}^a W^{b\sigma\nu} W_{\nu\mu}^a W^{b\mu\rho} + \frac{c_{16}}{\Lambda^4} B_{\rho\sigma} B^{\sigma\nu} W_{\nu\mu}^a W^{a\mu\rho} ,\end{aligned}\quad (3)$$

see eq. (5) below.

The explicit expression for dimension-8 Lagrangian in a broken phase (in which it is expressed in terms of the physical fields W^\pm , Z and $F_{\mu\nu}$) can be found, for instance, in [10]. We are interested in an effective Lagrangian for the anomalous $\gamma\gamma\gamma\gamma$ couplings. It is given by the formula [10]

$$\mathcal{L}_{\text{QNGC}}^{\gamma\gamma\gamma\gamma} = \zeta_1 F_{\mu\nu} F^{\mu\nu} F_{\rho\sigma} F^{\rho\sigma} + \zeta_2 F_{\mu\nu} F^{\nu\rho} F_{\rho\sigma} F^{\sigma\mu} ,\quad (4)$$

where

$$\begin{aligned}\zeta_1 &= [c_w^4 c_8 + s_w^4 c_9 + c_w^2 s_w^2 (c_{10} + c_{11})] \Lambda^{-4} , \\ \zeta_2 &= [c_w^4 c_{13} + s_w^4 c_{14} + c_w^2 s_w^2 (c_{15} + c_{16})] \Lambda^{-4} .\end{aligned}\quad (5)$$

The QGCs are actively studied for a long time. The anomalous $WWZZ$ vertex was probed at the LEP [12] (see also [13]) and Tevatron [14] colliders. The L3 Collaboration also searched for the $WWZZ$ couplings [15]. There have been investigations for the $\gamma\gamma W^+W^-$ couplings at the LHC in [16]-[23]. The possibility of measuring the $\gamma\gamma ZZ$ couplings were studied in [16]-[19], [10], and [24]. Recently, the LHC experimental bounds on QGCs have been presented by the CMS [25] and ATLAS [26] Collaborations. In a number of theoretical papers, search limits for the QGCs at future electron-proton colliders have been estimated [27]-[29]. The anomalous QGCs can be also probed at linear e^+e^- colliders [30], in particular, in the $e\gamma$ mode [31, 32] or $\gamma\gamma$ mode [33]-[34]. Finally, in [35, 36] the anomalous quartic couplings of the $\gamma\gamma ZZ$ vertex at the Compact Linear Collider (CLIC) [37, 38] have been examined.

The great potential of the CLIC in probing new physics is well-known [39]-[41]. At the CLIC, it is possible to investigate not only e^+e^- scattering but also $e\gamma$ and $\gamma\gamma$ collisions with real photons. In the present paper, we will examine the possibility of searching for anomalous $\gamma\gamma\gamma\gamma$ couplings in the light-by-light (LBL) scattering with ingoing Compton backscattered (CB)

photons at the CLIC. Both unpolarized and polarized initial photons will be considered. The first evidence of the process $\gamma\gamma \rightarrow \gamma\gamma$ was observed by the ATLAS and CMS Collaborations in high-energy ultra-peripheral PbPb collisions [42, 43]. The LBL collisions at the LHC have been studied in [44, 45]. Recently, the LBL scattering at the CLIC induced by axion-like particles has been examined [46, 47].

2 Light-by-light scattering in effective field theory

The e^+e^- colliders may operate in $e\gamma$ and $\gamma\gamma$ modes [48]. Hard real photon beams at the CLIC can be generated by the laser Compton backscattering. When soft laser photons collide with electron beams, a large flux of photons, with a great amount of the parent electron energy, is produced. Let E_0 and λ_0 be the energy and helicity of the initial laser photon beam, while E_e and λ_e be the energy and helicity of the electron beam before CB. In our calculations, two sets of these helicities, with opposite sign of λ_e , will be considered, namely

$$\begin{aligned}(\lambda_e^{(1)}, \lambda_0^{(1)}; \lambda_e^{(2)}, \lambda_0^{(2)}) &= (1, -0.8; 1, -0.8), \\(\lambda_e^{(1)}, \lambda_0^{(1)}; \lambda_e^{(2)}, \lambda_0^{(2)}) &= (1, +0.8; 1, +0.8),\end{aligned}\tag{6}$$

where the superscripts 1 and 2 enumerate the beams. The helicity of the photon with energy E_γ obtained by the Compton backscattering of the laser photons with helicity λ_0 off the electron beam is given by the formula

$$\xi(E_\gamma, \lambda_0) = \frac{\lambda_0(1-2r)[1-x+1/(1-x)] + \lambda_e r \zeta [1+(1-x)(1-2r)^2]}{1-x+1/(1-x)-4r(1-r)-\lambda_e \lambda_0 r \zeta (2r-1)(2-x)},\tag{7}$$

where $x = E_\gamma/E_e$, $r = x/\zeta(1-x)$, $\zeta = 4E_e E_0/m_e^2$, m_e being the electron mass.

The spectrum of the CB photons is defined by the helicities λ_0 , λ_e and dimensionless variables x , r , ζ as follows

$$\begin{aligned}f_{\gamma/e}(x) &= \frac{1}{g(\zeta)} \left[1-x + \frac{1}{1-x} - \frac{4x}{\zeta(1-x)} + \frac{4x^2}{\zeta^2(1-x)^2} \right. \\&\quad \left. + \lambda_0 \lambda_e r \zeta (1-2r)(2-x) \right],\end{aligned}\tag{8}$$

where

$$g(\zeta) = g_1(\zeta) + \lambda_0 \lambda_e g_2(\zeta) , \quad (9)$$

$$g_1(\zeta) = \left(1 - \frac{4}{\zeta} - \frac{8}{\zeta^2}\right) \ln(\zeta + 1) + \frac{1}{2} + \frac{8}{\zeta} - \frac{1}{2(\zeta + 1)^2} , \quad (10)$$

$$g_2(\zeta) = \left(1 + \frac{2}{\zeta}\right) \ln(\zeta + 1) - \frac{5}{2} + \frac{1}{\zeta + 1} - \frac{1}{2(\zeta + 1)^2} . \quad (11)$$

The maximum possible value of x is equal to

$$x_{\max} = \frac{(E_\gamma)_{\max}}{E_e} = \frac{\xi}{(1 + \xi)} . \quad (12)$$

The laser beam energy is chosen to maximize the backscattered photon energy E_γ . This can be achieved if one puts $\xi \simeq 4.8$, then $x_{\max} \simeq 0.83$.

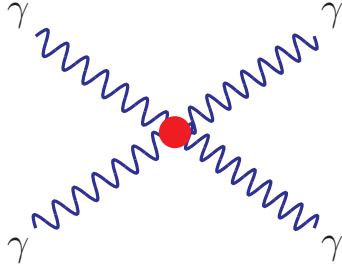


Figure 1: The diphoton production in the collision of the backscattered photons at the CLIC via anomalous quartic coupling.

The LBL scattering of the CB photons happens as shown in Fig. 1. Its differential cross section is expressed in terms of the CB photon spectra, their

helicities, and helicity amplitudes [49]

$$\begin{aligned}
\frac{d\sigma}{d\cos\theta} &= \frac{1}{128\pi s} \int_{x_{1\min}}^{x_{1\max}} \frac{dx_1}{x_1} f_{\gamma/e}(x_1) \int_{x_{2\min}}^{x_{2\max}} \frac{dx_2}{x_2} f_{\gamma/e}(x_2) \\
&\times \left\{ \left[1 + \xi \left(E_\gamma^{(1)}, \lambda_0^{(1)} \right) \xi \left(E_\gamma^{(2)}, \lambda_0^{(2)} \right) \right] \right. \\
&\quad \times (|M_{++++}|^2 + |M_{++--}|^2) \\
&\quad + \left[1 - \xi \left(E_\gamma^{(1)}, \lambda_0^{(1)} \right) \xi \left(E_\gamma^{(2)}, \lambda_0^{(2)} \right) \right] \\
&\quad \left. \times (|M_{+--+}|^2 + |M_{-+-+}|^2) \right\}, \tag{13}
\end{aligned}$$

where $x_1 = E_\gamma^{(1)}/E_e$ and $x_2 = E_\gamma^{(2)}/E_e$ are the energy fractions of the CB photon beams, $x_{1\min} = p_\perp^2/E_e^2$, $x_{2\min} = p_\perp^2/(x_1 E_e^2)$, p_\perp is the transverse momentum of the outgoing photons. \sqrt{s} is the center of mass energy of the e^+e^- collider, while $\sqrt{s x_1 x_2}$ is the center of mass energy of the backscattered photons. We will apply the cut on the rapidity of the final state photons $|\eta| < 2.5$.

The physical potential of linear e^+e^- colliders may be enhanced if the polarized beams are used [50, 51]. As will be seen below, it is exactly so in our case. For comparison, similar results for unpolarized electron beams will also be presented. Our calculations have shown that the total cross sections are almost indistinguishable from the SM ones for $\sqrt{s} = 380$ GeV (the first energy stage of the CLIC). That is why, we will focus on the energies $\sqrt{s} = 1500$ GeV (the second energy stage of the CLIC) and $\sqrt{s} = 3000$ GeV (the third energy stage of the CLIC). The expected integrated luminosities for these baseline CLIC energy stages [51] are presented in Tab. 1.

		$\lambda_e = 0$	$\lambda_e = -0.8$	$\lambda_e = +0.8$
Stage	\sqrt{s} , GeV	\mathcal{L} , fb $^{-1}$	\mathcal{L} , fb $^{-1}$	\mathcal{L} , fb $^{-1}$
2	1500	2500	2000	500
3	3000	5000	4000	1000

Table 1: The CLIC energy stages and integrated luminosities for the unpolarized and polarized initial electron beams.

We have calculated the differential cross sections $d\sigma/dp_t$, where p_t is the transverse momenta of the outgoing photons, see Figs. 2-5. To reduce the SM

background, we have imposed the cut on the invariant mass of the outgoing photons, $W = m_{\gamma\gamma} > 200$ GeV. The dips on these figures around $p_t \simeq 60$ GeV comes from the SM and interference terms. The reason is that the SM amplitudes include the t^{-1} term, t being the momentum transfer squared, while the contribution to the EFT terms comes mainly from medium and high p_t regions.

It is interesting to analyze the shapes of the curves corresponding to different values of the electron beam helicity λ_e . Let us consider the case ($\zeta_1 = 10^{-13}$ GeV $^{-4}$, $\zeta_2 = 0$) first. The differential cross sections with $\lambda_e = 0.8$ (blue curves) become dominant if $p_t > 300$ GeV for both energies. As for the cross section with $\lambda_e = -0.8$ (red curve), it exceeds the unpolarized cross section (black curve) at medium values of p_t , but become subdominant and decreasing at large p_t , for both values of \sqrt{s} . The situation for ($\zeta_1 = 10^{-14}$ GeV $^{-4}$, $\zeta_2 = 0$) is quite different. For $\sqrt{s} = 1500$ GeV, the cross section with $\lambda_e = -0.8$ exceeds other cross sections at medium values of p_t , while at large p_t , the cross section with $\lambda_e = 0.8$ becomes to dominate. For $\sqrt{s} = 3000$ GeV, the cross section with $\lambda_e = 0.8$ is the biggest one, starting from $p_t = 600$ GeV.

For the couplings ($\zeta_1 = 0, \zeta_2 = 10^{-13}$ GeV $^{-4}$), the cross sections are shown in the left panels of in Figs. 4-5. If $\sqrt{s} = 1500$ GeV, the differential cross section with $\lambda_e = -0.8$ ($\lambda_e = 0.8$) exceeds other ones for medium (large) values of p_t . For higher energy $\sqrt{s} = 3000$ GeV, the cross sections are close to each other up to $p_t = 750$ GeV. At larger p_t , the cross section with the helicity $\lambda_e = 0.8$ dominates. Finally, for ($\zeta_1 = 0, \zeta_2 = 10^{-14}$ GeV $^{-4}$) the differential cross sections do not significantly descend from ones obtained for ($\zeta_1 = 10^{-14}$ GeV $^{-4}$, $\zeta_2 = 0$), especially if $\sqrt{s} = 1500$ GeV is taken.

The results of our calculations of the total cross sections $\sigma(p_t > p_{t,\min})$, where $p_{t,\min}$ is the minimal transverse momentum of the outgoing photons, are shown in Figs. 6-9. The calculations have been made for two values of the CLIC energy, and two sets of the couplings (ζ_1, ζ_2), using $W = m_{\gamma\gamma} > 200$ GeV. Figs. 6, 7 demonstrate that for ($\zeta_1 = 10^{-13}$ GeV $^{-4}$, $\zeta_2 = 0$), $\lambda_e = 0.8$, and $\sqrt{s} = 1500(3000)$ GeV, the total cross section is approximately one order (two orders) of magnitude larger than the SM one. If ($\zeta_1 = 10^{-14}$ GeV $^{-4}$, $\zeta_2 = 0$), $\lambda_e = 0.8$, and $\sqrt{s} = 3000$ GeV, the value of the total cross section is comparable with the SM prediction for small $p_{t,\min}$. At the same time, the SM cross section decreases rapidly as $p_{t,\min}$ grows, while the total cross section remains almost unchanged up to $p_{t,\min} \simeq 1000$ GeV. For ($\zeta_1 = 10^{-14}$ GeV $^{-4}$, $\zeta_2 = 0$), $\lambda_e = 0.8$, and $\sqrt{s} = 1500$ GeV, the difference

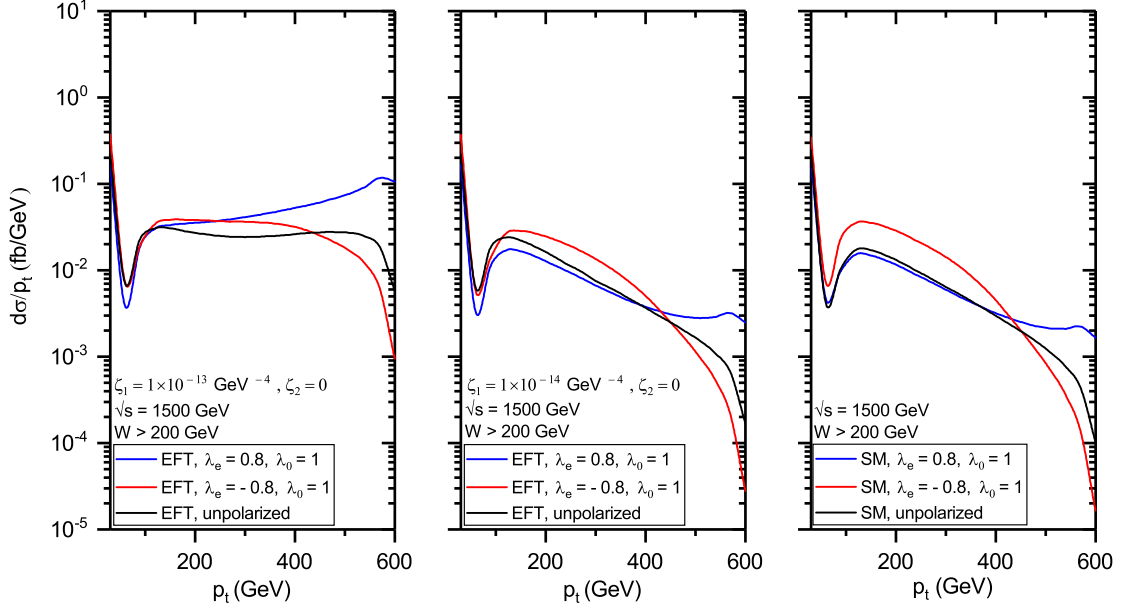


Figure 2: The differential cross sections for the process $\gamma\gamma \rightarrow \gamma\gamma$ as functions of transverse momenta of the outgoing photons for the e^+e^- collider energy $\sqrt{s} = 1500$ GeV with coupling values $\zeta_1 = 10^{-13}$ GeV $^{-4}$, 10^{-14} GeV $^{-4}$, $\zeta_2 = 0$.

between the total and SM cross sections are rather small. The same is true for $(\zeta_1 = 0, \zeta_2 = 10^{-13}$ GeV $^{-4})$, and $\sqrt{s} = 1500$ GeV. But for this set of ζ_1, ζ_2 , and larger collision energy $\sqrt{s} = 3000$ GeV, the total cross section is almost two orders of magnitude larger than the SM one, see Fig. 9.

It is interesting to examine a possible dependence of the total cross sections on a sign of the electron beam helicity λ_e , and to compare two polarized cases ($\lambda_e = \pm 0.8$) with the unpolarized one ($\lambda_e = 0$). Without a doubt, the value $\lambda_e = 0.8$ is the preferable one, either for $(\zeta_1 = 10^{-13}$ GeV $^{-4}, \zeta_2 = 0)$ or $(\zeta_1 = 0, \zeta_2 = 10^{-13})$ GeV $^{-4}$, no matter which values of energy is used. It remains true for $(\zeta_1 = 10^{-14}$ GeV $^{-4}, \zeta_2 = 0)$ and $(\zeta_1 = 0, \zeta_2 = 10^{-14})$ GeV $^{-4}$, if $\sqrt{s} = 3000$ GeV. For $\sqrt{s} = 1500$ GeV, that is so in the region $p_{t,\min} > 300$ GeV only.

Now let the electron beam helicity to have an opposite sign, $\lambda_e = -0.8$. If $(\zeta_1 = 10^{-13}$ GeV $^{-4}, \zeta_2 = 0)$, the polarized LBL cross section dominates

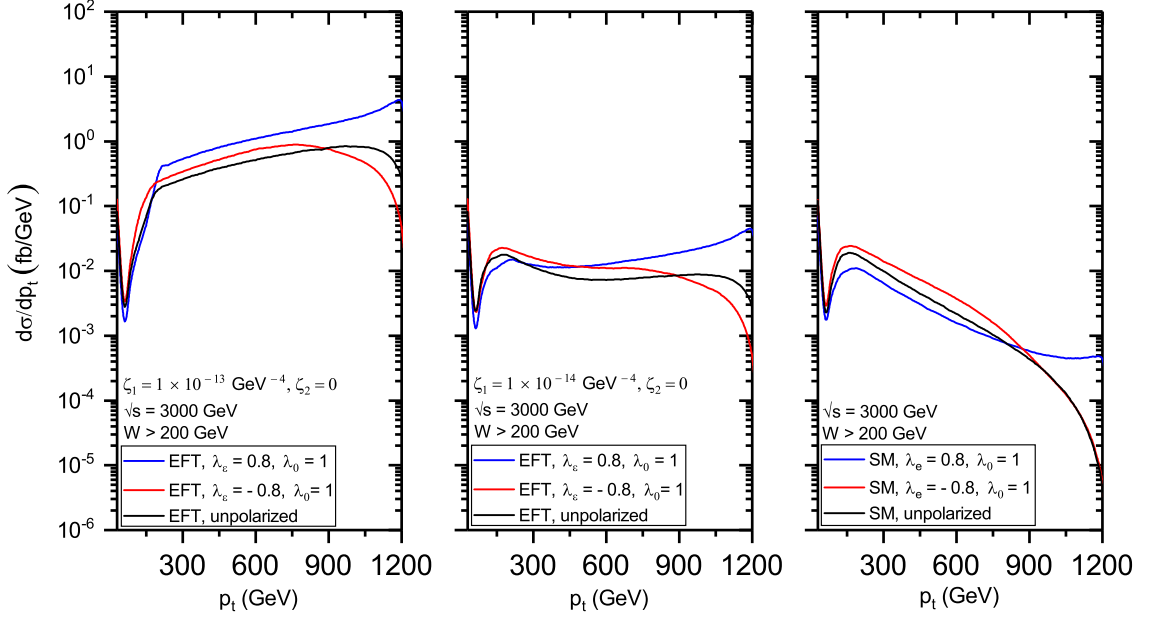


Figure 3: The differential cross sections for the process $\gamma\gamma \rightarrow \gamma\gamma$ as functions of transverse momenta of the outgoing photons for the e^+e^- collider energy $\sqrt{s} = 3000$ GeV with coupling values $\zeta_1 = 10^{-13}$ GeV $^{-4}$, 10^{-14} GeV $^{-4}$, $\zeta_2 = 0$.

for $\sqrt{s} = 1500$ GeV, regardless of $p_{t,\min}$. On the contrary, the values of the polarized and unpolarized cross sections are almost the same in the region $p_{t,\min} < 550$ GeV for $\sqrt{s} = 3000$ GeV, but for larger $p_{t,\min}$, the unpolarized cross section begins to dominate the polarized one. If the set of couplings ($\zeta_1 = 10^{-14}$ GeV $^{-4}$, $\zeta_2 = 0$) are considered for $\sqrt{s} = 1500$ GeV, the polarized cross section with $\lambda_e = -0.8$ is larger than the unpolarized cross section for $p_{t,\min} < 400$ GeV. For $\sqrt{s} = 3000$ GeV, the unpolarized cross section is almost indistinguishable from the polarized cross section in the region $p_{t,\min} < 450$ GeV, but it becomes to dominate as $p_{t,\min}$ grows. All these statements are illustrated by Figs. 6, 7.

For the case $\zeta_1 = 0$, the situation is different. For $\zeta_2 = 10^{-13}$ GeV $^{-4}$, and $\sqrt{s} = 1500$ GeV, the polarized cross section with $\lambda_e = -0.8$ is somewhat larger than the unpolarized cross section in the region $p_{t,\min} < 300$ GeV, as one can see in Figs. 8. For $\zeta_2 = 10^{-13}$ GeV $^{-4}$ and $\sqrt{s} = 3000$ GeV, the

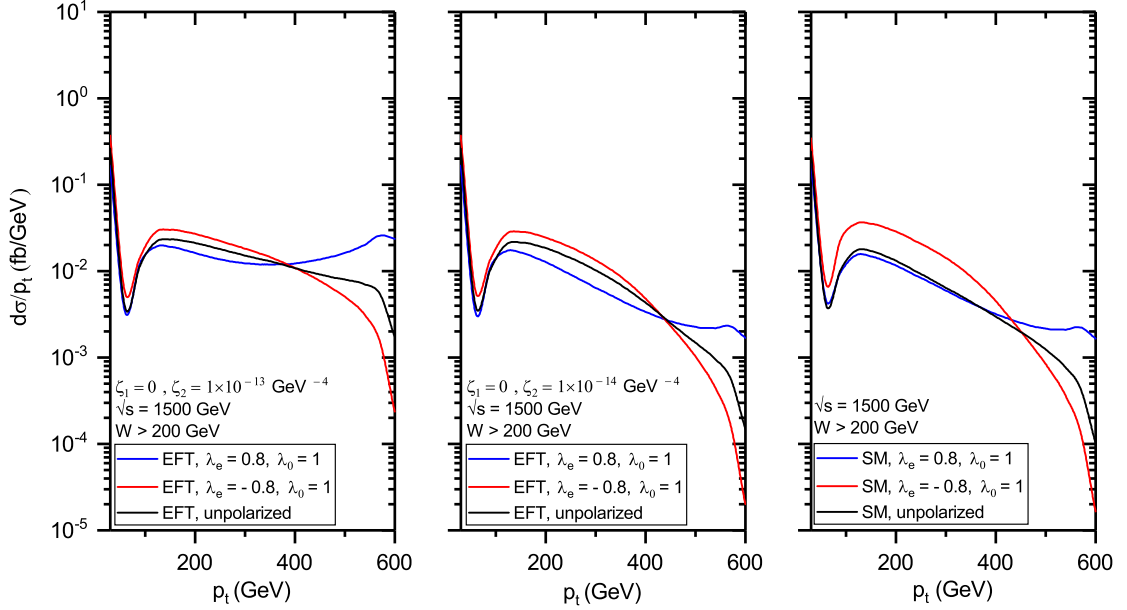


Figure 4: The same as in Fig. 2, but for $\zeta_1 = 0$, and $\zeta_2 = 10^{-13} \text{ GeV}^{-4}$, $10^{-14} \text{ GeV}^{-4}$.

unpolarized cross sections dominates the polarized one with $\lambda_e = -0.8$ for all $p_{t,\min}$, especially for $p_{t,\min} > 750 \text{ GeV}$, see Fig. 9. Analogously, for $\zeta_2 = 10^{-14} \text{ GeV}^{-4}$, the cross section with $\lambda_e = -0.8$ slightly exceeds the unpolarized one in the region $p_{t,\min} < 400 \text{ GeV}$ for $\sqrt{s} = 1500 \text{ GeV}$, as it is clear from Figs. 8. For larger values of $p_{t,\min}$, the unpolarized total cross exceeds the polarized one. As for the energy $\sqrt{s} = 3000 \text{ GeV}$, in the region $p_{t,\min} > 450 \text{ GeV}$, the unpolarized cross sections decreases very slowly, while the cross section corresponding to $\lambda_e = -0.8$ falls off rapidly.

It is clear from Figs. 6-9 that the total cross section deviation from the SM gets higher, as the cut $p_{t,\min}$ grows. Especially for $\lambda_e = 0.8$, and $\zeta_{1,2} = 10^{-13} \text{ GeV}^{-4}$, the total cross sections remain almost unchanged despite increasing $p_{t,\min}$. Therefore, large $p_{t,\min}$ could be used to obtain better sensitivity bounds on the couplings ζ_1 and ζ_2 . Note, however that for $\lambda_e = 0.8$, the CLIC expected integrated luminosities are four times smaller than for $\lambda_e = -0.8$, for both values of e^+e^- collision energy, see Tab. 1.

The pure EFT, interference and SM total cross sections $\sigma(p_t > 500 \text{ GeV})$

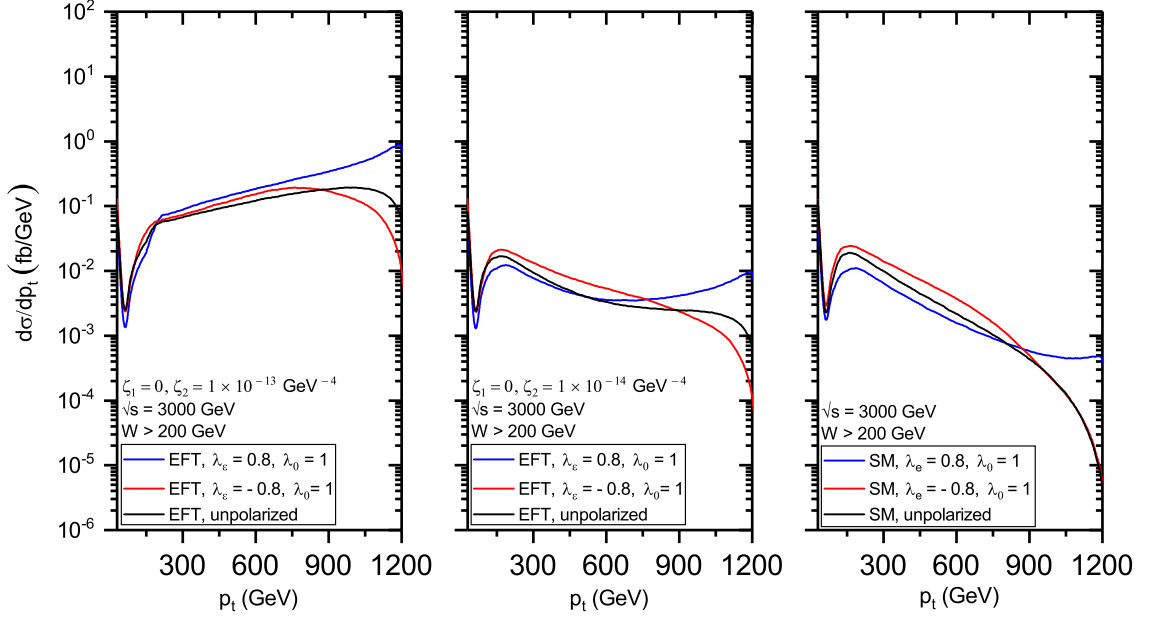


Figure 5: The same as in Fig. 3, but for $\zeta_1 = 0$, and $\zeta_2 = 10^{-13} \text{ GeV}^{-4}$, $10^{-14} \text{ GeV}^{-4}$.

for the couplings ($\zeta_1 = 10^{-13} \text{ GeV}^{-4}$, $\zeta_2 = 0$) are collected in Tabs. 2-3. We may conclude that the interference terms can be neglected. The number of the background events B is known and large (provided the integrated luminosities are taken from Tab. 1). We assume that the background uncertainty is negligible. To calculate the exclusion region, we use the following formula for the statistical significance (SS) [52]

$$SS = \sqrt{2[(S - B \ln(1 + S/B))]} , \quad (14)$$

where S is the number of signal events. We define the regions $SS \leq 1.645$ as the regions that can be excluded at the 95% C.L.

Our 95% C.L. exclusion regions for the couplings ζ_1, ζ_2 for the unpolarized LBL scattering are shown in Figs. 10, 11 with the cuts $W > 200 \text{ GeV}$, $p_t > 500 \text{ GeV}$. Note that for the unpolarized process the pure EFT cross section is proportional to the coupling combination $48\zeta_1^2 + 40\zeta_1\zeta_2 + 11\zeta_2^2$ [54]. As a result, the exclusion regions are ellipses rotated counterclockwise in the plane (ζ_1, ζ_2) through the angle $0.5 \arctan(80/37) \simeq 32.6^\circ$ about the origin.

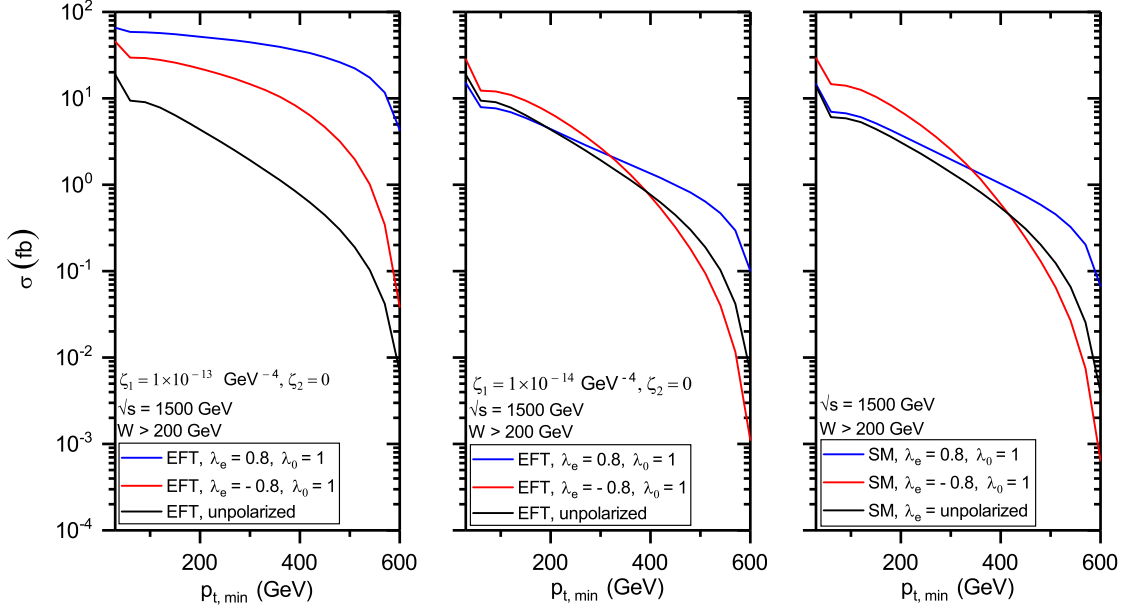


Figure 6: The total cross sections for the process $\gamma\gamma \rightarrow \gamma\gamma$ as functions of minimal transverse momenta of the outgoing photons for the e^+e^- collider energy $\sqrt{s} = 1500$ GeV with and coupling values $\zeta_1 = 10^{-13}$ GeV $^{-4}$, 10^{-14} GeV $^{-4}$, $\zeta_2 = 0$.

For the polarized LBL scattering at the CLIC, exclusion bounds on the anomalous photon couplings are presented in Tabs. 4, 5 using the cuts $W > 200$ GeV and $p_t > 500$ GeV. Note that values of the expected integrated luminosities depend on the energy \sqrt{s} . We see that for $\sqrt{s} = 1500$ GeV, the best limits take place for the initial electron beam helicity $\lambda_e = -0.8$, both for the ζ_1 and ζ_2 couplings. The bounds for the helicity $\lambda_e = +0.8$ and unpolarized scattering are close to each other. For the higher energy $\sqrt{s} = 3000$ GeV, the strongest (the weakest) limits are obtained for the LBL scattering with $\lambda_e = +0.8$ ($\lambda_e = -0.8$).

Previously, the discovery potential for the LBL scattering at the 14 TeV LHC has been estimated in [11], [53, 54]. As was shown in [53], the 14 TeV LHC 95% C.L. exclusion limits on ζ_1 and ζ_2 couplings are 1.5×10^{-14} GeV $^{-4}$ and 3.0×10^{-14} GeV $^{-4}$, respectively, for $L = 300$ fb $^{-1}$ integrated luminosity. For $L = 3000$ fb $^{-1}$ (high luminosity LHC), the values are twice smaller,

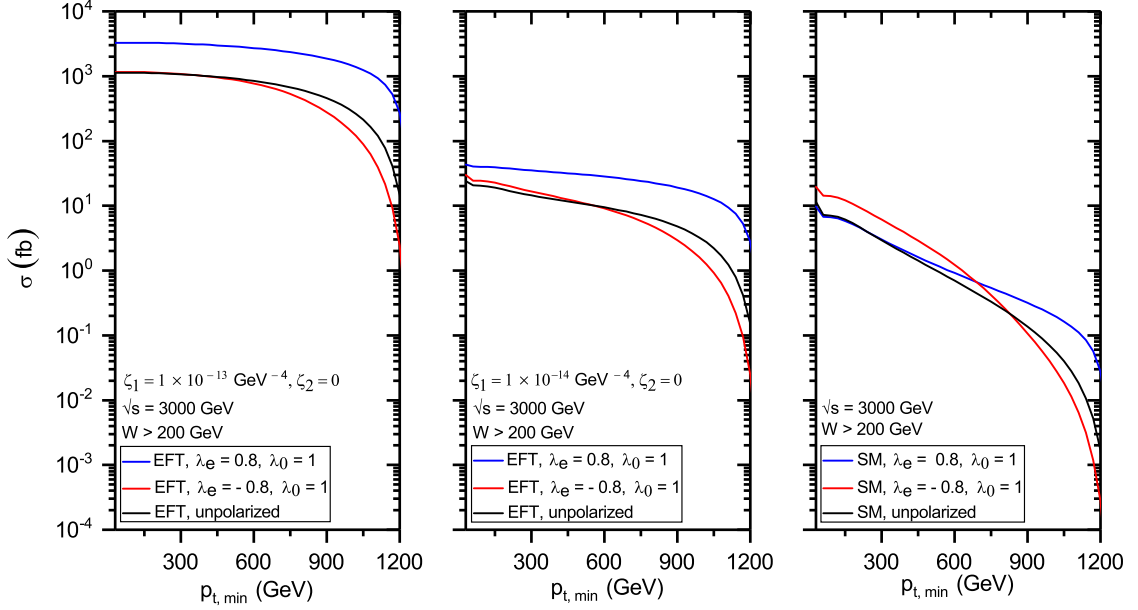


Figure 7: The total cross sections for the process $\gamma\gamma \rightarrow \gamma\gamma$ as functions of minimal transverse momenta of the outgoing photons for the e^+e^- collider energy $\sqrt{s} = 3000$ GeV with coupling values $\zeta_1 = 10^{-13}$ GeV $^{-4}$, 10^{-14} GeV $^{-4}$, $\zeta_2 = 0$.

7.0×10^{-15} GeV $^{-4}$ and 1.5×10^{-14} GeV $^{-4}$. The sensitivity in the (ζ_1, ζ_2) plane is shown in Fig. 12 taken from [54]. As one can see from Tabs. 4,5, our CLIC bounds on the couplings ζ_1, ζ_2 for the unpolarized LBL scattering with $\sqrt{s} = 1500$ GeV are approximately 1.2 times stronger than the LHC bounds obtained for the integrated luminosity $L = 3000$ fb $^{-1}$ [54]. The difference is even more pronounced for the unpolarized LBL scattering with $\sqrt{s} = 3000$ GeV, when our lower bounds on ζ_1, ζ_2 are approximately one order of magnitude smaller than the LHC lower bounds. The difference between the CLIC and LHC exclusion bounds becomes larger for the polarized LBL scattering.

In [36] the CLIC 95% C.L. sensitivity bounds on the coefficients f_{T_0}/Λ^4 and f_{T_9}/Λ^4 in the EFT Lagrangian (equivalent to the coefficients c_9/Λ^4 and c_{13}/Λ^4 in (3)) for $\sqrt{s} = 3000$ GeV and $L = 2000$ fb $^{-1}$ are presented. Note that these coefficients are only parts of our couplings ζ_1 and ζ_2 (5). The

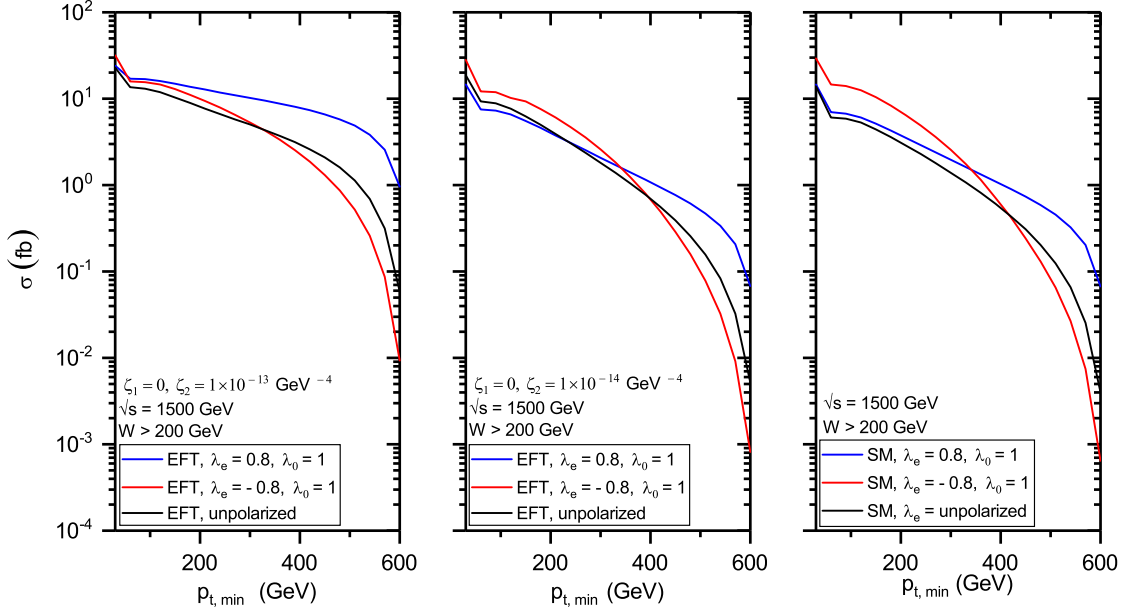


Figure 8: The same as in Fig. 6, but for $\zeta_1 = 0$, and $\zeta_2 = 10^{-13} \text{ GeV}^{-4}$, $10^{-14} \text{ GeV}^{-4}$.

bounds have been obtained by examining the anomalous quartic couplings of $ZZ\gamma\gamma$ vertex.

3 Conclusions

In the present paper, we have examined the anomalous quartic neutral couplings of the $\gamma\gamma\gamma\gamma$ vertex in the polarized light-by-light collisions of the Compton backscattered photons at the CLIC. Both the second and third stages of the CLIC are considered with the collision energies $\sqrt{s} = 1500 \text{ GeV}$ and $\sqrt{s} = 3000 \text{ GeV}$, respectively. The helicity of the initial electron beam was taken to be $\lambda_e = \pm 0.8$. The unpolarized case ($\lambda_e = 0$) has been also considered. We used the $SU(2)_L \times U(1)_Y$ effective Lagrangian describing the contribution to the anomalous quartic neutral gauge boson couplings. Its part, relevant to the anomalous $\gamma\gamma\gamma\gamma$ vertex (4), expressed in terms of the physical fields, contains two couplings ζ_1 , ζ_2 of dimension -4 .

We have calculated both the differential cross sections and total cross

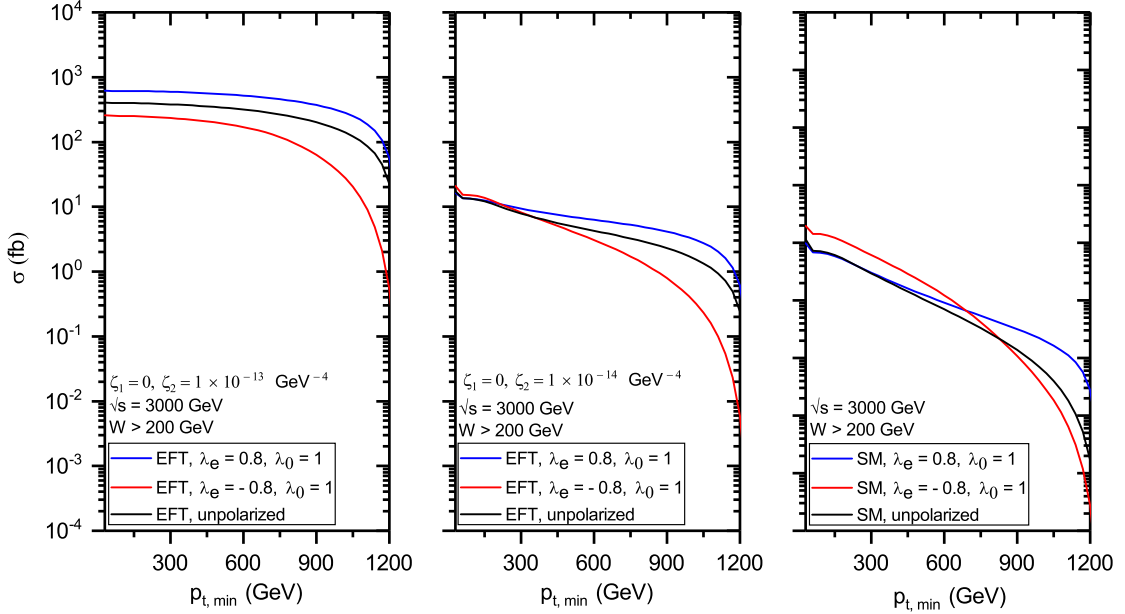


Figure 9: The same as in Fig. 7, but for $\zeta_1 = 0$, and $\zeta_2 = 10^{-13} \text{ GeV}^{-4}$, $10^{-14} \text{ GeV}^{-4}$.

sections of the light-by-light scattering $\gamma\gamma \rightarrow \gamma\gamma$. We have tested the following possibilities: i) ζ_1 is equal to $10^{-13} \text{ GeV}^{-4}$ or $10^{-14} \text{ GeV}^{-4}$, $\zeta_2 = 0$; ii) $\zeta_1 = 0$, ζ_2 is equal to $10^{-13} \text{ GeV}^{-4}$ or $10^{-14} \text{ GeV}^{-4}$. The differential cross sections are shown in Figs. 2-5. For comparison, in the right panels of these figures, the SM cross sections for the same helicities of the electron beams are shown. The LBL scattering with $\lambda_e = 0.8$ has appeared to be dominant in the range $p_t > 300 \text{ GeV}$ for both values of \sqrt{s} , if $\zeta_1 = 10^{-13} \text{ GeV}^{-4}$, $\zeta_2 = 0$. When $\zeta_1 = 0$, $\zeta_2 = 10^{-13} \text{ GeV}^{-4}$ it dominates in the high p_t region only, $p_t > 400(750) \text{ GeV}$, for $\sqrt{s} = 1500(3000) \text{ GeV}$. The differential cross sections with the helicity $\lambda_e = -0.8$ dominates in the region $p_t = 100 - 400 \text{ GeV}$, only if the couplings $\zeta_1 = 10^{-14} \text{ GeV}^{-4}$ or $\zeta_2 = 10^{-14} \text{ GeV}^{-4}$ and $\sqrt{s} = 1500 \text{ GeV}$ are considered.

The total cross sections are presented in Figs. 6-9 as functions of the minimal transverse momenta of the outgoing photons $p_{t,\min}$. For the couplings $\zeta_1 = 10^{-13} \text{ GeV}^{-4}$, $\zeta_2 = 0$, the cross sections of the LBL scattering with the helicity $\lambda_e = 0.8$ are significantly larger than the cross sections of the LBL

	$\lambda_e = 0$	$\lambda_e = -0.8$	$\lambda_e = +0.8$
Cross sections	σ , fb	σ , fb	σ , fb
Pure EFT	4.61	2.22	7.48
Interference	0.066	0.031	0.10
SM	0.158	0.083	0.49

Table 2: The pure EFT, interference and SM contributions to the total cross sections for $\sqrt{s} = 1500$, $W > 200$ GeV, $p_t > 500$ GeV and $\zeta_1 = 10^{-13}$ GeV $^{-4}$, $\zeta_2 = 0$.

	$\lambda_e = 0$	$\lambda_e = -0.8$	$\lambda_e = +0.8$
Cross sections	σ , fb	σ , fb	σ , fb
Pure EFT	932	896	2901
Interference	2.56	2.02	2.54
SM	1.21	2.22	1.32

Table 3: The same as in Tab. 2, but for $\sqrt{s} = 3000$.

scattering with the opposite helicity $\lambda_e = -0.8$ and unpolarized cross sections. The figures demonstrate us that the total cross section deviation from the SM gets higher, as $p_{t,\min}$ increases. The effect is most pronounced for $\sqrt{s} = 3000$ GeV and couplings $\zeta_1 = 10^{-13}$ GeV $^{-4}$, $\zeta_2 = 0$. For $\zeta_{1,2} = 10^{-14}$ GeV $^{-4}$, the EFT cross sections exceed the SM one for all values of $p_{t,\min}$, only if the collision energy is equal to 3000 GeV, and the helicity λ_e is either 0.8 or zero. For $\zeta_{1,2} = 10^{-14}$ GeV $^{-4}$ and lower energy $\sqrt{s} = 3000$ GeV, the values of the total cross sections are comparable with the SM cross sections. Note that the cross sections are more sensitive to the coupling ζ_1 than to the coupling ζ_2 .

The CLIC sensitivity bounds on ζ_1 and ζ_2 , coming from the process $\gamma\gamma \rightarrow \gamma\gamma$, have been calculated for two values of the collision energy \sqrt{s} and three values of the initial beam helicity λ_e (unpolarized case included). For the unpolarized LBL scattering at the CLIC, the 95% C.L. exclusion regions are shown in Figs. 10, 11. Our results for the polarized LBL scattering are presented in Tabs. 4, 5. For the e^+e^- collision energy $\sqrt{s} = 3000$ GeV, our lower bounds on ζ_1, ζ_2 have appeared to be approximately one order of magnitude stronger than the corresponding LHC bounds obtained for $\sqrt{s} = 14$ TeV and integrated luminosity $L = 3000$ fb $^{-1}$ in [54], even for the unpolarized case. The difference becomes larger, if one considers the polar-

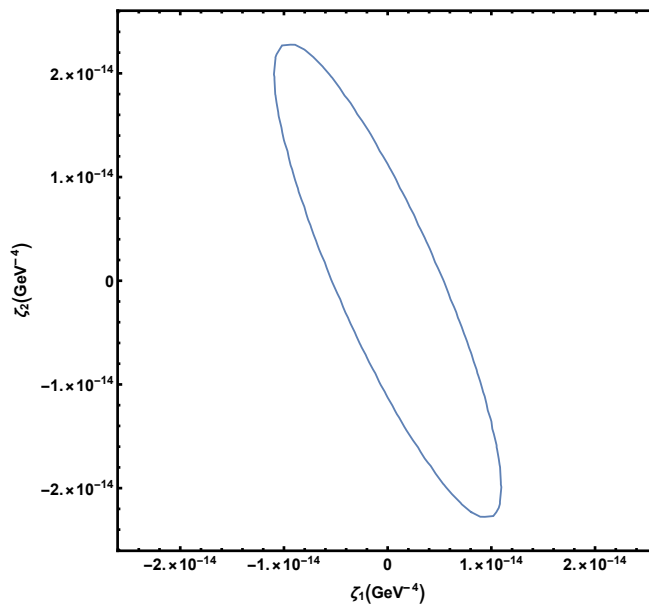


Figure 10: The 95% C.L. exclusion region for the couplings (ζ_1, ζ_2) for the unpolarized light-by-light scattering at the CLIC. The collision energy is $\sqrt{s} = 1500$ GeV, the integrated luminosity is $L = 2500 \text{ fb}^{-1}$, $W > 200$ GeV and $p_t > 500$ GeV.

ized LBL scattering at the CLIC with $\sqrt{s} = 3000$ GeV and $\lambda_e = 0.8$, see the fourth column in Tab. 5. All said above allows us to conclude that the LBL scattering at the CLIC has a great physical potential in searching for the anomalous quartic neutral couplings of the $\gamma\gamma\gamma\gamma$ vertex.

References

- [1] W. Buchmuller and D. Wyler, *Effective lagrangian analysis of new interactions and flavour conservation*, Nucl. Phys. B **268**, 621 (1986).
- [2] K. Hagiwara, R.D. Peccei, D. Zeppenfeld and K. Hikasa, *Probing the Weak Boson Sector in $e^+e^- \rightarrow W^+W^-$* , Nucl. Phys. B **282**, 253 (1987).
- [3] S. Godfrey, *Quartic Gauge Boson Couplings*, in *Proceedings of the International symposium on Vector Boson Self-Interactions*, AIP Conf. Proc.

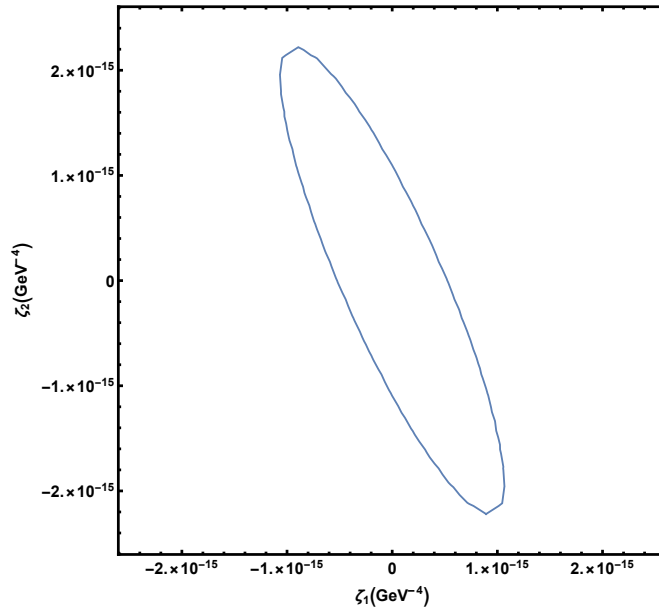


Figure 11: The same as in Fig. 10, but for $\sqrt{s} = 3000$ GeV and $L = 5000$ fb $^{-1}$.

No 350, AIP, NY, 1995 [arXiv:hep-ph/9505252].

- [4] G. Balanger and F. Boudjema, $\gamma\gamma \rightarrow W^+W^-$ and $\gamma\gamma \rightarrow ZZ$ as tests of novel quartic couplings, Phys. Lett. B. **288**, 210 (1992).
- [5] W.J. Stirling and A. Werthenbach, *Anomalous Quartic Couplings in $\nu\bar{\nu}\gamma\gamma$ Production via WW -Fusion at LEP2*, Phys. Lett. B **466**, 369 (1999); W.J. Stirling and A. Werthenbach, *Anomalous Quartic Couplings in $W^+W^-\gamma$, $Z^0Z^0\gamma$ and $Z^0\gamma\gamma$ Production at Present and Future e^+e^- Colliders*, Eur. Phys. J. C **14**, 103 (2000).
- [6] A. De Rújula, M.B. Gavela, P. Hernandez and E. Massó, *The Self-couplings of Vector Bosons: does LEP-1 obviate LET-2?*, Nucl. Phys. B **384**, 3 (1992).
- [7] K. Hagiwara, S. Ishihara, R. Szalapski and D. Zeppenfeld, *Low-energy constraints on electroweak three gauge boson couplings*, Phys. Lett. B **283**, 353 (1992); *Low energy effects of new interactions in the electroweak boson sector*, Phys. Rev. D **48**, 2182 (1993).

Helicity	0	-0.8	+0.8
Luminosity, fb ⁻¹	2500	2000	500
ζ_1 , GeV ⁻⁴ ($\zeta_2 = 0$)	5.41×10^{-15}	4.25×10^{-15}	6.71×10^{-15}
ζ_2 , GeV ⁻⁴ ($\zeta_1 = 0$)	1.13×10^{-14}	7.86×10^{-15}	1.31×10^{-14}

Table 4: The 95% C.L. exclusion limits on the couplings ζ_1 and ζ_2 for the CLIC collision energy $\sqrt{s} = 1500$ GeV, and the cuts $W > 200$ GeV and $p_t > 500$ GeV.

Helicity	0	-0.8	+0.8
Luminosity, fb ⁻¹	5000	4000	1000
ζ_1 , GeV ⁻⁴ ($\zeta_2 = 0$)	5.26×10^{-16}	9.07×10^{-16}	4.58×10^{-16}
ζ_2 , GeV ⁻⁴ ($\zeta_1 = 0$)	1.10×10^{-15}	1.72×10^{-15}	9.37×10^{-16}

Table 5: The same as in Tab. 4, but for $\sqrt{s} = 3000$ GeV.

- [8] C. Degrande *et al.*, *Effective Field Theory: A Modern Approach to Anomalous couplings*, Ann. Phys. **335**, 21 (2013).
- [9] O.J.P. Éboli, M.C. Gonzalez-Garcia and J.K. Mizukoshi, *$pp \rightarrow jje^\pm\mu^\pm\nu\nu$ and $jje^\pm\mu^\mp\nu\nu$ at $\mathcal{O}(\alpha_{\text{em}}^6)$ and $\mathcal{O}(\alpha_{\text{em}}^4\alpha_s^2)$ for the study of the quartic electroweak gauge boson vertex at CERN LHC*, Phys. Rev. D **74**, 073005 (2006).
- [10] R.S. Gupta, *Probing quartic gauge boson couplings using diffractive photon fusion at the LHC*, Phys. Rev. D **85**, 014006 (2012).
- [11] S. Fichet and G. von Gersdorff, *Anomalous gauge couplings from composite Higgs and warped extra dimensions*, JHEP **03**, 102 (2014).
- [12] P. Achand *et al.* (L3 Collaboration), *Study of the $W^+W^-\gamma$ process and limits on anomalous quartic gauge boson couplings at LEP*, Phys. Lett. B **527**, 29 (2002); A. Heister *et al.* (ALEPH Collaboration), *Constraints on anomalous QGC's in e^+e^- interactions from 183-GeV to 209-GeV*, Phys. Lett. B **602**, 31 (2004); G. Abbiendi *et al.* (OPAL Collaboration), *A study of $W^+W^-\gamma$ events at LEP*, Phys. Lett. B **580**, 17 (2004); J. Abdallah *et al.* (DELPHI Collaboration), *Measurement of the $e^+e^- \rightarrow W^+W^-\gamma$ cross-section and limits on anomalous quartic gauge couplings with DELPHI*, Eur. Phys. J. C **31**, 139 (2003).

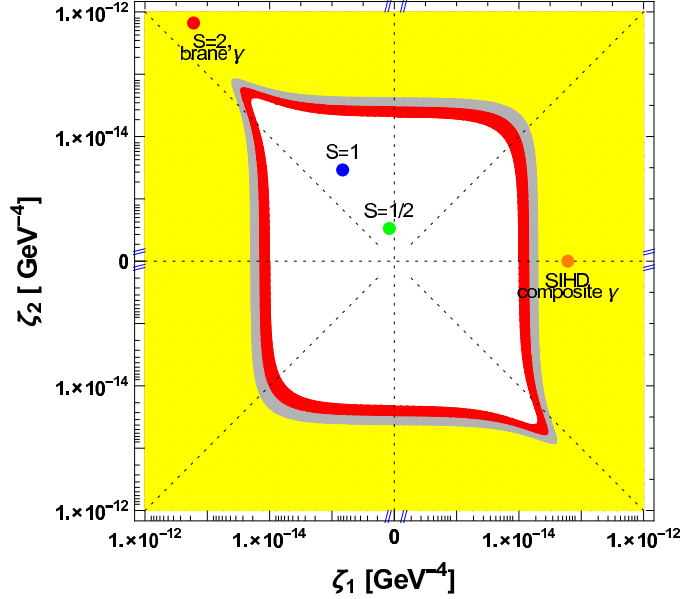


Figure 12: The LHC sensitivity in the (ζ_1, ζ_2) plane. In particular, the red region can be probed at the 95% C.L. using proton tagging at the LHC. The white region is inaccessible. The figure is taken from Ref. [54].

- [13] G. Bélanger *et al.*, *Bosonic quartic couplings at LEP-2*, Eur. Phys. J. C **13**, 283 (2000).
- [14] V.M. Abazov *et al.* (D0 Collaboration), *Search for anomalous quartic $WW\gamma\gamma$ couplings in dielectron and missing energy final states in $\bar{p}p$ collisions at $\sqrt{s} = 1.96$ TeV*, Phys. Rev. D **88**, 012005 (2013).
- [15] P. Achand *et al.* (L3 Collaboration), *The $e^+e^- \rightarrow Z\gamma\gamma \rightarrow q\bar{q}\gamma\gamma$ reaction at LEP and constraints on anomalous quartic gauge boson couplings*, Phys. Lett. B **540**, 43 (2002).
- [16] O.J.P. Éboli, M.C. Gonzalez-Garcia, S.M. Lietti and S.F. Novaes, *Anomalous Quartic Gauge Boson Couplings at Hadron Colliders*, Phys. Rev. D **63**, 075008 (2001); O.J.P. Éboli, M.C. Gonzalez-Garcia and S.M. Lietti, *Bosonic quartic couplings at CERN LHC*, Phys. Rev. D **69**, 095005 (2004).

- [17] T. Pierzchała and K. Piotrkowski, *Sensitivity to anomalous quartic gauge couplings in photon-photon interactions at the LHC*, Nucl. Phys. B. Proc. Suppl. **179**, 257 (2008).
- [18] E. Chapon, O. Kepka and C. Royon, *Probing $WW\gamma\gamma$ and $ZZ\gamma\gamma$ quartic anomalous couplings with 10 pb^{-1} at the LHC*, arXiv:0908.1061; E. Chapon, C. Royon and O. Kepka, *Anomalous quartic $WW\gamma\gamma$, $ZZ\gamma\gamma$, and trilinear $WW\gamma$ couplings in two-photon processes at high luminosity at the LHC*, Phys. Rev. D **81**, 074003 (2010).
- [19] A. Senol, *Anomalous quartic $WW\gamma\gamma$ and $ZZ\gamma\gamma$ couplings in γp collision at the LHC*, Int. J. Mod. Phys. A **29**, 1450148 (2014).
- [20] G. Perez, M. Sekulla and D. Zeppenfeld, *Anomalous quartic gauge couplings and unitarization for the vector boson scattering process $pp \rightarrow W^+W^+jjX \rightarrow l^+\nu_l l^+\nu_l jjX$* , Eur. Phys. J. C **78**, 759 (2018).
- [21] Yu-Chen Guo, Ying-Ying Wang, Ji-Chong Yang and Chong-Xing Yue, *Constraints on anomalous quartic gauge couplings via $W\gamma jj$ production at the LHC*, arXiv:2002.03326.
- [22] S. Tizchang and S. M. Etesami, *Pinning down the gauge boson couplings in $WW\gamma$ production using forward proton tagging*, arXiv:2004.12203.
- [23] Jian-Wen Zhu, Ren-You Zhang, Wen-Gan Ma, Q. Yang and Yi Jiang, *$W^+W^-\gamma$ production at hadron colliders with NLO QCD+EW corrections and parton shower effects*, J. Phys. G: Nucl. Part. Phys. **47**, 055006 (2020).
- [24] İ. Şahin and B. Şahin, *Anomalous quartic $ZZ\gamma\gamma$ couplings in gamma-proton collision at the LHC*, Phys. Rev. D **86**, 115001 (2012).
- [25] A.M. Sirunyan *et al.* (CMS Collaboration), *Measurement of the cross section for electroweak production of a Z boson, a photon and two jets in proton-proton collisions at $\sqrt{s} = 13\text{ TeV}$ and constraints on anomalous quartic couplings*, JHEP **06**, 076 (2020).
- [26] G. Aad *et al.* (ATLAS Collaboration), *Measurements of $Z\gamma$ and $Z\gamma\gamma$ production in pp collisions at $\sqrt{s} = 8\text{ TeV}$ with the ATLAS detector*, Phys. Rev. D **93**, 112002 (2006).

- [27] V. Ari, A. Gutiérrez-Rodríguez, M.A. Hernández-Ruiz and M. Köksal, *Anomalous quartic $W^+W^-\gamma\gamma$ couplings in e^-p collisions at the LHeC and the FCC-he*, Eur. Phys. J. Plus **135**, Article number: 336 (2020).
- [28] V. Ari, E. Gurkanli, A.A. Billur and M. Köksal, *Model independent study for the anomalous quartic $WW\gamma\gamma$ couplings at Future Electron-Proton Colliders*, Nucl. Phys. B **957**, 115102 (2020).
- [29] A. Gutierrez-Rodríguez, M.A. Hernández-Ruiz, E. Gurkanli, V. Ari and M. Köksal, *Study on the anomalous quartic $W^+W^-\gamma\gamma$ couplings of electroweak bosons in e^-p collisions at the LHeC and the FCC-he*, arXiv:2005.11509.
- [30] A. Denner, S. Dittmaier, M. Roth and D. Wackerroth, *Probing anomalous quartic gauge-boson couplings via $e^+e^- \rightarrow 4$ fermions + γ* , Eur. Phys. J. C **20**, 201 (2001).
- [31] O.J.P. Éboli, M.C. Gonzalez-Garcia and S.F. Novaes, *Quartic anomalous couplings in $e\gamma$ colliders*, Nucl. Phys. B **411**, 381 (1994).
- [32] S. Atağ and İ. Şahin, *Anomalous Quartic $WW\gamma\gamma$ and $ZZ\gamma\gamma$ couplings in $e\gamma$ collision with initial beams and final state polarizations*, Phys. Rev. D **75**, 073003 (2007).
- [33] O.J.P. Éboli and J. K. Mizukoshi, *Probing anomalous quartic couplings in $e\gamma$ and $\gamma\gamma$ colliders*, Phys. Rev. D **64**, 075011 (2001).
- [34] İ. Şahin, *Anomalous quartic $WW\gamma\gamma$ and $WWZ\gamma$ couplings through W^+W^-Z production in $\gamma\gamma$ collisions*, J. Phys. G: Nucl. Part. Phys. **36**, 075007 (2009).
- [35] M. Köksal, *Anomalous quartic $ZZ\gamma\gamma$ couplings at the CLIC*, Eur. Phys. J. Plus **130**, Article number: 75 (2015).
- [36] M. Köksal, V. Ari and A. Senol, *Search for Anomalous Quartic $ZZ\gamma\gamma$ Couplings in Photon-Photon Collisions*, Advances in High Energy Physics **2016**, Article ID: 8672391 (2016).
- [37] H. Braun *et al.* (CLIC Study Team), *CLIC 2008 parameters*, CERN-OPEN-2008-021, CLIC-NOTE-764.

- [38] M.J. Boland *et al.* (CLIC and CLICdp Collaborations), *Updated baseline for a staged Compact Linear Collider*, CERN-2016-004, arXiv:1608.07537.
- [39] D. Dannheim *et al.*, *CLIC e^+e^- Linear Collider Studies*, in *Proceedings of 2013 Community Summer Study on the Future of U.S. Particle Physics: Snowmass on the Mississippi (CSS2013)*, 29 July – 6 August, 2013, MN, US (arXiv:1208.1402).
- [40] *The CLIC Potential for New Physics*, eds. J. de Blas *et al.*, CERN Yellow report: Monographs, Vol. 3/2018, CERN-2018-009-M (CERN, Geneva, 2018).
- [41] R. Franceschini, *Beyond the Standard Model physics at CLIC*, Int. J. Mod. Phys. A **35**, 2041015 (2020).
- [42] M. Aaboud *et al.* (ATLAS Collaboration), *Evidence for light-by-light scattering in heavy-ion collisions with the ATLAS detector at the LHC*, Nat. Phys. **13**, 852 (2017); G. Aad *et al.* (ATLAS Collaboration), *Observation of Light-by-Light Scattering in Ultrapерipheral Pb + Pb Collisions with the ATLAS Detector*, Phys. Rev. Lett. **123**, 052001 (2019).
- [43] D. d’Enterria *et al.* (CMS Collaboration), *Evidence for light-by-light scattering in ultraperipheral PbPb collisions at $\sqrt{s} = 5.02$ TeV*, Nucl. Phys. A **982**, 791 (2019).
- [44] S. Atağ, S.C. İnan and İ. Şahin, *Extra dimensions in $\gamma\gamma \rightarrow \gamma\gamma$ process at the CERN-LHC*, JHEP **09**, 042 (2010).
- [45] S.C. İnan and A.V. Kisselev, *Probe of the Randall-Sundrum-like model with the small curvature via light-by-light scattering at the LHC*, Phys. Rev. D **100**, 095004 (2019).
- [46] S.C. İnan and A.V. Kisselev, *A search for axion-like particles in light-by-light scattering at the CLIC*, JHEP **06**, 183 (2020).
- [47] S.C. İnan and A.V. Kisselev, *Polarized light-by-light scattering at the CLIC induced by axion-like-particles*, arXiv:200.01693.
- [48] I.F. Ginzburg, G.L. Kotkin, V.G. Serbo and V.I. Telnov, *Colliding γe and $\gamma\gamma$ beams based on the single-pass e^+e^- colliders (of VLEPP*

- Type*), Nucl. Instrum. Meth. **205**, 47 (1983); I.F. Ginzburg, G.L. Kotkin, S.L. Panfil, V.G. Serbo and V.I. Telnov, *Colliding γe and $\gamma\gamma$ beams based on single-pass e^+e^- accelerators II. Polarization effects, monochromatization improvement, *ibid.* **219**, 5 (1984).*
- [49] O. Çakir, K.O. Ozansoy, *Unparticle searches through gamma-gamma scattering*, Eur. Phys. J. C **56**, 279 (2008).
- [50] G. A. Moortgat-Pick *et al.*, *The role of polarised positrons and electrons in revealing fundamental interactions at the Linear Collider*, Phys. Rep. **460**, 131 (2008).
- [51] R. Franceschini, P. Roloff, U. Schnoor and A. Wulzer, *The Compact Linear e^+e^- Collider (CLIC): Physics Potential*, arXiv:1812.07986.
- [52] G. Cowan, K. Cranmer, E. Gross and O. Vitells, *Asymptotic formulae for likelihood-based tests of new physics*, Eur. Phys. J. C **71**, 1554 (2011).
- [53] S. Fichtel *et al.*, *Probing new physics in diphoton production with proton tagging at the Large Hadron collider*, Phys. Rev. D **89**, 114004 (2014).
- [54] S. Fichtel *et al.*, *Light-by-light scattering with intact protons at the LHC: from standard model to new physics*, JHEP **02**, 165 (2015).